PHYSICAL REVIEW B VOLUME 15, NUMBER 4 15 FEBRUARY 1977

Size and shape effects in light scattering from small silver, copper, and gold particles*

J. D. Eversole† and H. P. Broida
Physics Department and Quantum Institute, University of California, Santa Barbara, California 93106
(Received 22 March 1976)

Spectra of light scattered from small particles of silver, copper, and gold have been observed between 220 and 500 nm, and interpreted on the basis of size measurements of particle samples taken concurrently with the spectra. Particles were formed by homogeneous nucleation in a flowing inert gas bath containing vapor from the bulk metal. Mean particle diameters between 2 and 150 nm were measured by electron microscopy. A resonance peak was observed at 367 ± 5 nm (3.80 ± 0.06 eV) in the scattered light spectrum of silver particles, principally due to the collective oscillation of conduction electrons. An analysis of the scattered light resonance of silver particles was made using measured particle size distributions, and exact calculations of scattering from spheres including damping predicted by the free-electron gas model. Significant differences between observed spectra and calculations indicate that the width of the resonance is influenced by nonspherical shapes as well as by collisions of conduction electrons with the particle surface.

INTRODUCTION

Although the general characteristics of resonances in light extinction and scattering from small solid particles have been known since the 1900's,[1] detailed accounting for size and shape effects has not yet been accomplished. There is increasing interest in the dependence on particle size of the dielectric function of the material and other physical properties such as magnetic susceptibility, thermal conductivity, and lattice spacing. A major difficulty in experimentally addressing such questions lies in producing uniform particles, especially for materials which melt or evaporate at relatively high temperatures. This paper describes a method for the generation of uniform particles. Two specific advantages of the method are: (a) it uses a flow system and hence the particle size and shape distributions at any given point in the flow remain constant for long periods of time (minutes), and (b) the formation of particles from the vapor state in an inert gas facilitates sampling for electron microscopy.

Recently several workers have made studies of metallic particles formed by evaporation from the heated bulk metal in static, inert gas,[2-21] or by trapping particles from a flow system in a solid matrix.[22,23] Although many properties of these particles have been investigated, the optical properties in the visible region and the nucleation process itself have received little attention.

In this work, particles were formed in a flow apparatus which has been described previously.[24-26] The apparatus originally was used to produce large concentrations of atomic and diatomic sodium for spectroscopic study,[27] and it was discovered that under some conditions particles also were formed. After an initial study of light scattering from sodium particles,[28] improvements were made in the production of particles, and a survey of "plasma" resonance light scattering from the alkali metals was carried out.[24] Changes in positions and widths of the plasma resonances were interpreted on the basis of other work[29] as resulting from changes in the mean particle size. Attempts to directly measure the particle size distribution of alkali metals by electron microscopy were unsuccessful due to reactions with the atmosphere and melting in the electron beam. Following other workers[5,7,20] more stable, higher melting point metals such as zinc, cadmium, and manganese were used to form particles. These particles were amenable to investigation by electron microscopy[30] but did not exhibit strong characteristic structure in the scattered light spectrum.

Metals such as silver, copper, and gold have atomic electron structures similar to the alkali metals. The apparatus was modified to attain sufficiently high temperatures to use silver, copper, and gold[25,26] since it was conjectured that both electron microscopy and optical studies could be done with these metals. Results of experiments with these materials are reported in this paper.[26] Spectral structure in light scattering and absorption from silver and gold particles has been reported many times; however, in all previous experiments the particles were embedded in a dielectric medium which significantly shifted the optical structure.[31-38]

EXPERIMENTAL

Detailed descriptions of the apparatus have been presented elsewhere,[24-26,30] and only a general outline of the apparatus and its use is given here.

Particles are produced by evaporating bulk metal

in a heated flowing inert gas. The buffer gas carries metal vapor to cooler regions of the flow system where a supersaturated condition of the metal vapor is produced. At sufficiently low temperature, spontaneous condensation of small particles occurs. Electron microscopy shows particle sizes from 2 to 150 nm, depending on the production conditions and collection location in the system. Frequently particles have simple crystalline geometric shapes, usually hexagonal in cross section.

The experimental apparatus, shown in Fig. 1, consists of a furnace where the metal is heated and evaporated, and an observation chamber above the furnace where particles are formed, observed, and sampled. The observation chamber is a six-arm cross made of 10-cm diameter stainless-steel tubing.[25,26] Particles are formed in the observation chamber by appropriately adjusting the furnace temperature (via heater filament current), the nitrogen carrier gas flow (valve located below the furnace), and the pumping speed (throttle valve to the vacuum pump). Continuum light from

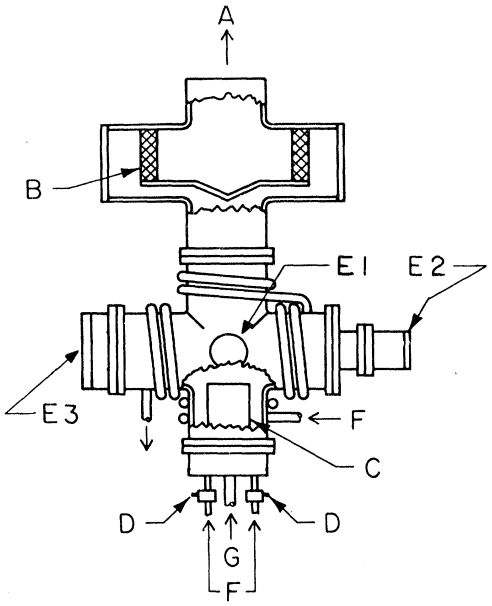

FIG. 1. Schematic diagram of vacuum flow system used to produce particles. The metal evaporation furnace is housed in the lower arm *F* of the water-cooled cross. Carrier gas enters at *G* and entrains the metal vapor formed in the furnace *C*. Current is supplied to the furnace with feed-throughs *D*. Light enters the chamber through window *E*1, illuminating the particles. Scattered light from the particles is observed by eye through window *E*3, and by a monochromator through window *E*2. Particles are carried up toward vacuum pump *A* and are trapped in filter *B*. Particle sampling apparatus is operated through a port located opposite to window *E*1.

a 150-W xenon arc lamp was directed into the observation chamber to illuminate particles so that they could be directly observed by eye. Opposite the visual observation window a $\frac{3}{4}$-m grating monochromator was situated about 10 cm from the third window; no lens was used between the monochromator and the observation region. Therefore, light scattered by the particles at right angles both to the incident beam and the flow direction of the particles was detected simultaneously by eye and through the monochromator.

Bulk metal was heated in an alumina crucible centered within a coiled tungsten resistance heating element. The heating element was surrounded by zirconia spun fiber thermal insulation.[25,26] Nitrogen gas was introduced at the bottom of the furnace and flowed around the crucible, entraining and carrying the metal vapor into the observation chamber. Flow rates of N_2 between 200 to 1000 μmoles/sec were used at gas pressures from 0.1 to 2 kPa (0.75 to 15 Torr).

In previous work with the alkali metals[24] it was possible to obtain particle nucleation in a laminar, unidirectional flow. However, for reasons not entirely understood, materials which require greater furnace temperatures nucleate only at high carrier gas flow rates of over 300 μmoles/sec. At these higher flow rates, swirling eddy currents develop around the central carrier gas stream. It is in the centers of these eddy currents that particles of silver, copper, and gold are observed. Electron microscopy of samples indicate that nucleation occurs near the boundary of the central flow and the eddy current. Attempts to modify the apparatus so that particle nucleation occurs in the unidirectional stream have been unsuccessful.

Samples for electron microscopy were obtained by allowing the particles to collect on a Parlodian plastic film supported by a 200-mesh copper grid attached to the end of a metal rod.[30] The rod could be positioned to collect particles at various points within the observation chamber and could be slid in and out of the observation region or sealed off with a valve. With the valve closed, the sampling apparatus could be removed and the coated grids changed. In this way successive particle samples were obtained without disturbing the rest of the system.

Scattered light spectra were taken at wavelengths between 220 and 500 nm by detection with a uv-sensitive photomultiplier tube. Amplified signals from the photomultiplier tube were recorded simultaneously by a strip chart and an analog magnetic tape recorder. Background spectra, obtained in the absence of particles, were recorded after every spectral scan to compensate for metal de-

position on the windows. Spectral data stored on the analog magnetic tape recorder were played back into a computer at a later time. The computer converted the analog signals into a one-dimensional array of integers representing spectral intensities at equally spaced intervals of 0.212 nm.

In reducing the data, scattered light spectra were computer corrected for background, instrument response, and lamp characteristics on a point-by-point basis. Eight-point smoothing was then applied to the corrected spectra, giving an effective resolution of ~2 nm, comparable to the monochromator resolution. Final spectra were then graphed on an incremental plotter interfaced to the computer.

RESULTS

A. Silver

Silver particles were observed with a minimum furnace current of about 34 A at 7.5 V, corresponding to a temperature of 1400 K as measured with an optical pyrometer. Furnace temperatures higher than about 1500 K produced unstable particle flows with large, macroscopic pieces of the material from the crucible being blown into the observation region. The major qualitative change as the furnace temperature increased was an increase in scattered light for the same pressure and flow rate.

At a flow rate of 360 μmoles/sec of nitrogen carrier gas, light scattering was not observed until the pressure was increased to 0.15 kPa. Particles were first seen in the centers of the eddy currents of N_2 on either side of the central flow stream. Under these conditions the scattered light appeared blue in color, with low intensity, and totally polarized perpendicular to the scattering plane. As the pressure was increased, the scattered light became more white, less plane polarized, and more intense. At 0.38 kPa the scattered light appeared faintly blue, and only about 10% plane polarized. On the basis of the dipole calculation of scattering from a sphere, the general characteristics of increasing intensity and decreasing polarization suggest that the particles were becoming larger as the pressure increased.

Spectra for all materials studied change most significantly as the chamber pressure changes. A resonance peak is the main spectral feature of the light scattered by silver particles. The position of this resonance peak gradually shifts to longer wavelengths as the pressure is increased (Fig. 2). The width of the resonance also becomes greater as the pressure increases, but it broadens in an asymmetric way toward longer wavelengths. The formation of particles occurs only for pressures between roughly 0.2–0.6 and 1.1–1.5 kPa. Therefore the pressure could not be set for equal pressure intervals in the presentation of the spectra in Fig. 2, and the apparent consistency in the way the spectra changed may be somewhat fortuitous. Similar changes in the resonance peaks occur as the furnace temperature is increased at a constant pressure, but the magnitude of change is much less than pressure-induced changes. Spectra taken with low furnace temperature were essentially identical to spectra taken with a higher furnace temperature but at lower chamber pressure.

Since the intensity of light scattered from particles decreases as the pressure is lowered, photo-

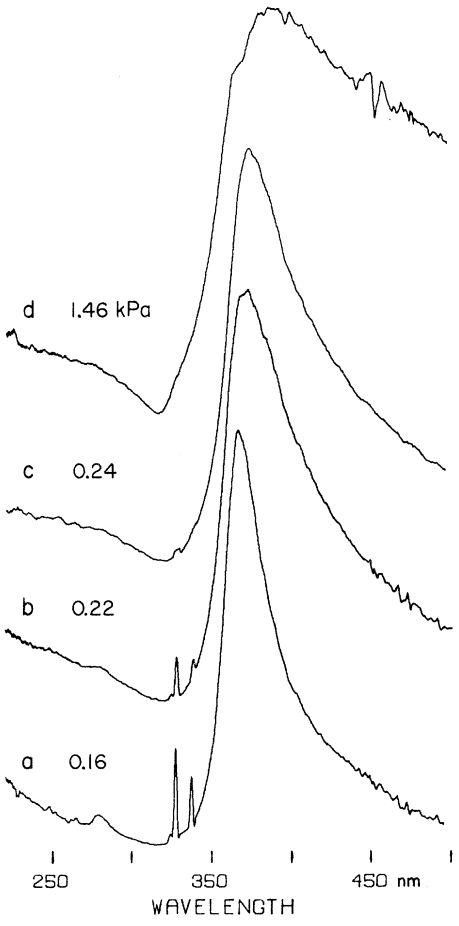

FIG. 2. Survey of observed scattered light intensity as a function of wavelength from silver particles. Spectra were obtained for four values of the chamber pressure, increasing from bottom to top as indicated by the numbers in the lower left corner of each spectrum. Carrier gas flow rate of 360 μmoles/sec and the furnace temperature remained constant. Spectra have been normalized to the same height and vertically offset for clarity.

luminescence from atomic lines becomes relatively greater. In Fig. 2 silver atom lines at 328.9 and 339.1 nm are seen. The small bump between 270 and 290 nm in the bottom spectrum is unresolved photoluminescence from Ag_2,[39] also observed during this work, particularly at low pressure.

The flow rate of nitrogen carrier gas had a strong effect on particle formation. Slowly increasing the flow from zero and keeping the pressure approximately constant (0.5 kPa), particles were not observed until a flow rate of 340 μmoles/sec was reached. By 400 μmoles/sec the particles has disappeared again and did not reappear until a flow rate of around 900 μmoles/sec was reached.

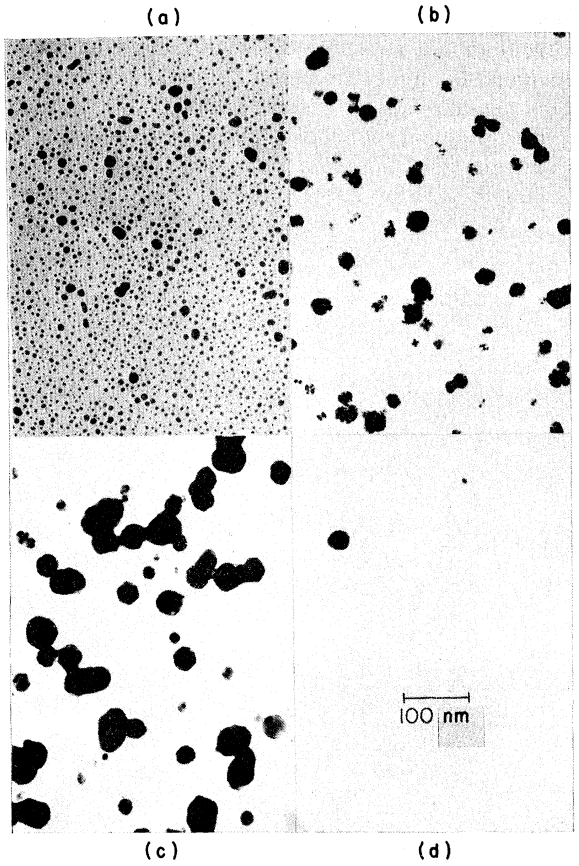

FIG. 3. Pressure dependence of samples of silver particles. Four samples were obtained under the same conditions as the spectra shown in Fig. 2, with (a) taken at the lowest pressure (0.09 kPa), (b) at 0.16 kPa, (c) at 0.31 kPa, and (d) at 0.99 kPa. Scale indicated in (d) applies to all four photographs. Samples were obtained at approximately the same location in the observation chamber from collection grids exposed for about 10 sec. Owing to the high contrast required for reproduction some of the smaller particles do not show up. Particles shown in (a) have rounded shapes because of a long period of storage in air.

Particles were seen at flow rates above 1000 μmoles/sec, but such conditions were avoided because of excessive turbulence. Spectra obtained from particles at a flow rate of 930 μmoles/sec showed no significant difference from spectra obtained with flow rates between 340 and 400 μmoles/sec. Changes in color, polarization, and intensity with variations in pressure appeared the same at 930 μmoles/sec flow rate as were described for lower flow rates. The only significant difference between the high- and low-flow-rate regimes was the spatial pattern of the particles in the observation chamber.

The hypothesis that changes in the spectra with increasing pressure are primarily due to increasing particle size (which was assumed in the earlier work with alkali metals[24]) was generally confirmed by electron microscopic measurement in the present study. Representative photographs of samples taken under conditions similar to those used to obtain the spectra in Fig. 2 are shown in Fig. 3 and changes in the size distribution with different pressures are clearly seen. Sampling difficulties existed for the somewhat turbulent flow pattern obtained at high pressures, and samples under these conditions were usually too poor to be informative.

Figure 4 is a histogram plotting the number of particles versus the average diameter of the particles. Particles were classified into groups having diameters larger than 100, 50–100, 25–50, 25–12.5, 12.5–6.25, and less than 6.25 nm. Parti-

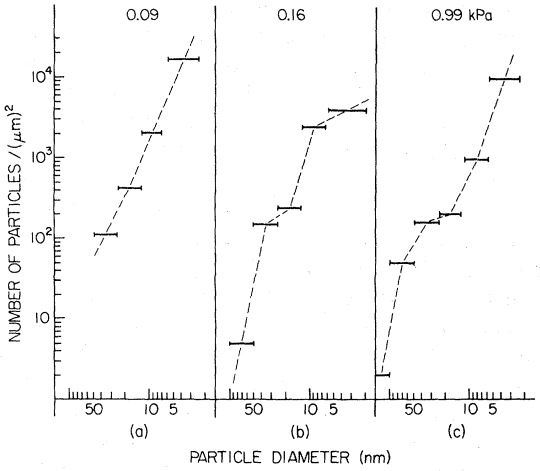

FIG. 4. Graphs of the number of particles counted from the photographs shown in Figs. 3(a)–3(d) for different size categories. Data are plotted on a log-log scale and dotted lines have been drawn between adjacent data bars of each sample to provide the numbers of particles at 5, 10, 20, 40, 60, 80, 100, and 120 nm diameters. Graphs (a), (b), and (c) correspond to the photographs of Figs. 3(a)–3(c), respectively.

cles smaller than 2.0 nm were not distinguishable. The graphs were plotted on a log-log scale to cover the large range in numbers and sizes.

Position in the observation chamber also was found to be a significant factor in size distribution. Generally, for samples taken closer to the furnace opening, larger particles were absent. Earlier work with electron microscopy of zinc particles[30] also showed that particle size increased with distance from the furnace opening, implying particle growth in time.

B. Copper and gold

Formation and observations of copper, gold, and silver particles were similar. The major differences were the greater furnace temperatures required to produce copper and gold vapors, and the fact that the resonance peaks for copper and gold occur at wavelengths shorter than 220 nm. For copper particles a typical operating current was 44 A at 11 V giving a furnace temperature of 1700 K. Gold particles were first observed at 53 A and 12.6 V giving a furnace temperature near 1900 K.

The flow patterns of copper and gold particles, their formation behavior as a function of flow rate, and their polarization, intensity, and formation characteristics as a function of pressure, were all very similar to those for silver particles. At low pressures with a flow rate of 360 μmoles/sec, scattered light from both gold and copper particles had a slight bluish color. Otherwise the copper and gold particles appeared white, and in general there was less light scattering in the visible region of the spectrum.

Figure 5 represents three normalized scattered light spectra from copper particles. The spectra have been corrected for instrument response, white-light characteristics, and background scattering. The primary spectral feature is a sharp rise toward shorter wavelength. It is important to realize that a peak in the scattering does not occur at 220 nm; calculations show that a peak does occur at still shorter wavelengths.

In Fig. 6, corrected scattered light spectra are shown for gold particles. The spectra are similar to copper particle spectra in that they indicate a resonance peak that occurs at wavelengths shorter

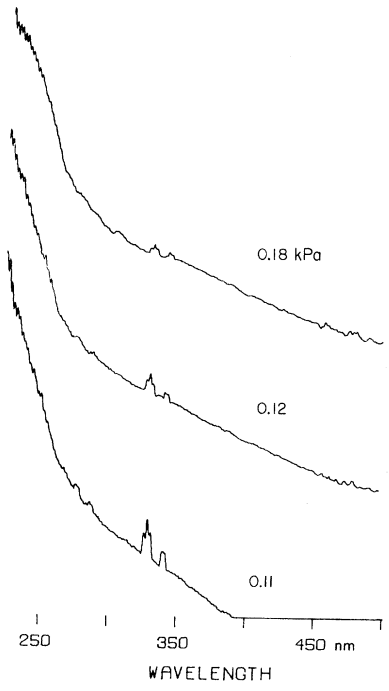

FIG. 5. Survey of scattered light spectra from copper particles. Spectra were obtained for three values of the chamber pressure, increasing from bottom to top as indicated by the numbers in the lower right corner of each spectrum. Carrier gas flow rate of 360 μmoles/sec and the furnace temperature remained constant. Spectra have been normalized to the same height and vertically offset for clarity.

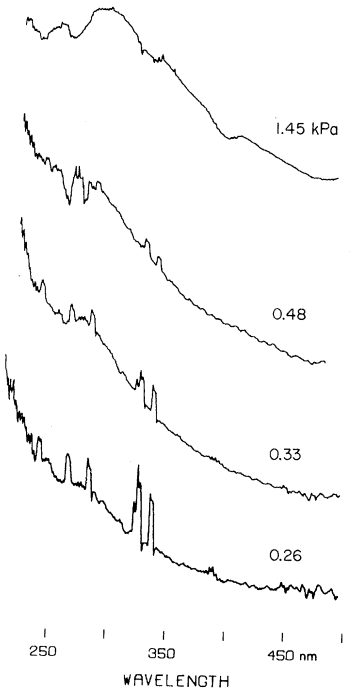

FIG. 6. Survey of scattered light spectra from gold particles. Spectra were obtained for four values of the chamber pressure increasing from bottom to top as indicated by the numbers in the lower right corner of each spectrum. Carrier gas flow rate of 360 μmoles/sec and the furnace temperature remained constant. Spectra have been normalized to the same height and vertically offset for clarity.

than 220 nm (with the exception of the top spectrum).

Qualitative features of the scattered light spectra from gold and copper particles followed similar patterns. The spectra exhibit a strong dependence on pressure that is consistent with the interpretation of a resonance peak at shorter wavelengths becoming broader. Various atomic resonance lines of gold and copper were recorded and they were generally more prominent at lower pressures and toward the center of the chamber (as with silver spectra). Since background spectra were obtained by turning off the N_2 carrier gas flow, photoluminescence from atomic species was observed frequently in the background spectra as well. The occurrence of what appears to be atomic line absorption in the spectrum of gold particles taken at 0.48 kPa is in fact caused by atomic gold lines that became stronger in the background spectrum.

Samples of copper and gold particles obtained for electron microscopy measurements reflected the same general patterns observed with silver particle samples. Particle size increased in samples taken with higher chamber pressures. For similar exposure times and experimental conditions samples of copper and gold particles appeared similar to samples of silver particles. No general qualitative or quantitative differences between the particle samples of the three materials were found.

ANALYSIS

A relatively simple way to understand resonant scattering and absorption in small particles is to consider a macroscopic model. The dipole scattering cross section (sca) of a dielectric sphere is[40]

$$c_{\text{sca}} = \tfrac{1}{4} d^2 \alpha^4 [(\tilde{\epsilon} - 1)/(\tilde{\epsilon} + 2)]^2 , \qquad (1)$$

where d is the sphere diameter, $\alpha = \pi d/\lambda$, and $\tilde{\epsilon} = \epsilon_1 + i\epsilon_2$ is the complex dielectric function. This expression is valid provided that retardation effects are small, or in the case of light scattering, that d is much smaller than the wavelength of light λ. If ϵ_1 happens to be equal to -2 (and ϵ_2 is small), then the scattering cross section can become quite large. Therefore, a first-order approximation predicts a scattering resonance at the wavelength region in which ϵ_1 is close to -2.

While the macroscopic approach is helpful it does not reveal the mechanism causing the resonant scattering. From the macroscopic point of view the physical mechanism for scattering is whatever contributes significantly to the polarizability of the material at a frequency where the real part of the dielectric constant has a value of -2. Since for some materials the real part of the dielectric constant as a function of frequency passes through the value -2 more than once, such particles would have more than one resonance, each with a different physical origin. Thus structure in the scattering and absorption spectra of small particles is caused by several different physical mechanisms[40] such as plasmons (free electrons), polaritons (lattice vibrations), and excitons (electron-hole pairs).

In going from the simple model to real particles three substantial obstacles appear: (i) particles will usually occur with a distribution of sizes rather than a single size, (ii) particles have irregular shapes, and (iii) the dielectric constant depends on particle size. The first two difficulties involve changes in the form of Eq. (1) to account for the (observable) distribution of sizes and shapes. However, the last obstacle is more fundamental since changes of the dielectric function with particle size are dependent on the physical mechanism. The size and shape distribution of particles produced on the experimental apparatus were directly observed in samples with an electron microscope (Fig. 3). For the most part, particle shapes were approximately spherical. This aspect will be discussed later, but in fact the theoretical treatment of shape effects for arbitrary sizes of particles becomes very difficult. Therefore, the approach used here is to calculate the relative scattered light intensity from a distribution of spheres conforming to the measured size distributions. For calculations, the dielectric constant of the bulk material was used. Hence, differences between observed and calculated spectra are attributed primarily to changes in the dielectric constant.

The first step in this analysis was to calculate the scattered light intensity from spheres of different diameters (usually referred to as Mie scattering). In previous calculations[29,41,42] the empirical values for the bulk-metal dielectric constant were fitted to the free-electron model. For the alkali metals such a fit is very accurate. For silver and gold particles embedded in water or glass this procedure also is appropriate since a surrounding dielectric medium will shift the particle resonances to longer wavelengths where the free-electron model is valid. For silver, gold, and copper particles in a vacuum, however, the particle resonances occur in an energy region where a significant contribution to the dielectric function comes from interband transitions and the method is not appropriate. Fortunately, recent index of refraction measurements on gold, copper, and silver[43,44] provide enough data to make a reasonable point-by-point calculation of particle scattering. No attempt was made to fit the data to a

continuous function. In regions where the particle scattering was changing rapidly, additional values of the dielectric function were obtained by linear interpolation. All calculations were carried out on an IBM 360 computer, and graphed on an incremental plotter. The quantity calculated (C) as a function of wavelength is the scattered light intensity at a scattering angle of 90° (I_{sca}) normalized to the incident intensity/nm (I_0). The quantity C is proportional to the differential scattering cross section[26,45,46]:

$$C = \frac{I_{sca}}{I_0} = \frac{|S_1|^2 + |S_2|^2}{1/\lambda^2} . \quad (2)$$

S_1 and S_2 are series of Ricatti-Bessel functions with Legendre polynomial coefficients and are implicit functions of the particle diameter d, the dielectric constant $\tilde{\epsilon}$, and λ.

Figures 7 and 8 illustrate calculations using Eq. (2) of scattering from spheres of copper and gold, respectively. Sphere diameters of 10, 20, 40, and 80 nm were chosen for both figures. Comparison of Figs. 7 and 8 with Figs. 5 and 6, respectively, indicates good agreement between the observed and calculated spectra. For all of these figures the individual spectra were plotted to the same wavelength scale, and normalized to the same height.

The calculations shown in Figs. 7 and 8 indicate a resonance peak occurring at shorter wavelengths than 200 nm for very small particles. As the particle size increases, the resonance peak shifts to longer wavelengths and becomes broader. These calculations confirm the experimental observations that variations in the observed scattered light spectra for carrier gas pressure changes were caused by changes in the particle size distribution of the samples. More detailed analysis is not possible because the entire resonance peak could not be recorded with present apparatus.

In the case of silver particles there was no difficulty, since the resonant peak occurs well within the accessible spectral range. Therefore, a more sophisticated method incorporating electron microscopic results with the spectral analysis was justified. Scattered light spectra were first calculated for various sized spheres in the same way as for copper and gold (Figs. 7 and 8) using the bulk values of the dielectric constant as a function of wavelength. These calculated spectra were then multiplied by a weighting factor proportional to the number of particles of the appropriate size found in a given sample, as in Fig. 4. Then the weighted spectra of a given sample were added together to give a synthesized spectrum to be compared to the

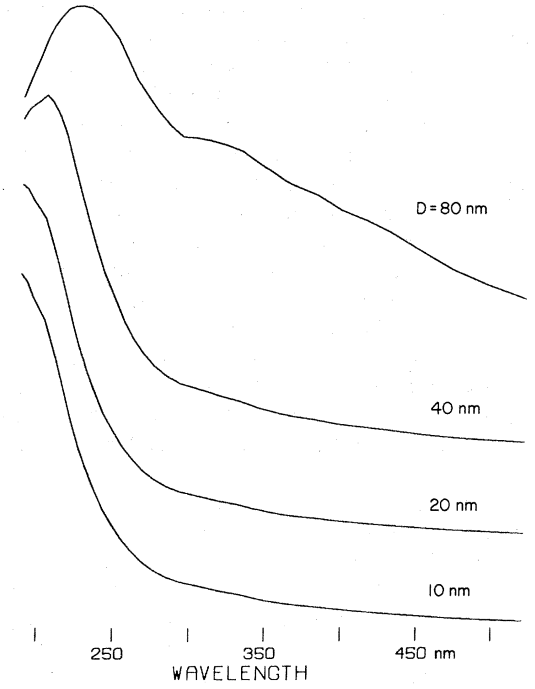

FIG. 7. Calculations of scattered light intensity from copper spheres of different sizes at a scattering angle of 90° over the wavelength region of 200–500 nm. Graphs for different sphere diameters have been normalized to the same height and vertically offset for clarity.

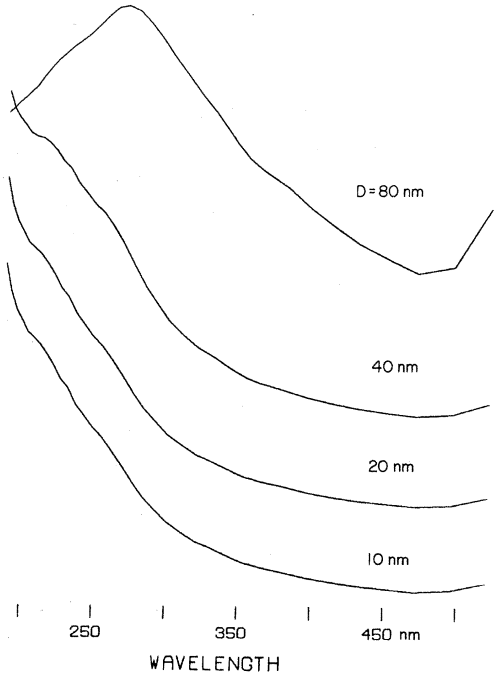

FIG. 8. Calculations of the scattered light intensity from gold spheres of different sizes at a scattering angle of 90° over the spectral region of 200–500 nm. As in Fig. 7 the graphs are normalized to the same height and vertically offset for clarity.

observed spectrum corresponding to the sample conditions. Figure 9 shows the results of adding the calculated spectra of various sized spheres according to the distributions shown in Fig. 4.

It is of interest to determine the relative intensity contribution of each particle size group to the total synthesized spectrum. Table I summarizes the relative numbers of various sized particles in three samples (shown in Figs. 3 and 4) whose calculated spectra are shown in Fig. 9 and indicates the relative contribution of each particle size to the synthesized spectrum. For each particle size group the calculated relative intensity of scattering per particle (at the spectral peak C_{max}) is multiplied by the number of particles present in that size range for each sample. The product represents the relative contribution to the spectrum.

All of the features of the observed spectra (Fig. 2) are evident in the synthesized spectra (Fig. 9). The maximum of the resonance shifts to longer wavelengths and the resonance broadens asymmetrically to longer wavelengths as the mean particle size increases. Even changes in the slope of the small rise at short wavelengths (220–320 nm) agrees with the observed spectra. It is evident that there is good agreement between the observed and calculated spectra. The actual position of the resonance peak is strongly dependent on the values of the real part of the index of refraction used in the calculation. Therefore, the agreement of observation and calculation is a confirmation of the accuracy of the previously measured optical constants.

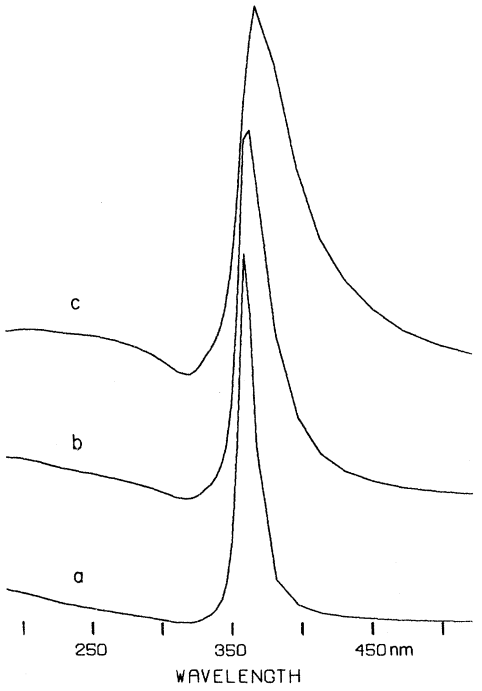

FIG. 9. Synthesized spectra for silver spheres obtained by adding together single sphere scattering calculations of different sphere diameters with weighting factors taken from the graphs shown in Fig. 4. Resulting synthesized spectra have been normalized to the same height and vertically offset. Wavelength scale and peak height are the same as for Fig. 2 so that comparison to the observed spectra corresponding to the same particle size distributions can be made. Contribution of each sphere size is indicated in Table I.

The major discrepancy between Figs. 2 and 9 is in the width of the resonance peaks, with the calculated spectra being somewhat sharper than the observed spectra. It was anticipated that some such deviation should exist with particles which are sufficiently small. The effect of the particle surface on the oscillation of electrons in the particle is analogous to a damping of the electrons' motion. Hence the oscillation amplitude at resonance will decrease as the particle size becomes small with a consequent increase in the half-width of the resonance curve.

A criterion for determining when the size of a particle is a dominant relaxation mechanism is expressed by

$$d = 2V_F\tau_0 , \tag{3}$$

where d is the particle diameter, V_F is the Fermi velocity, and τ_0 is the bulk relaxation time for a free electron. Using bulk values for the Fermi velocity and relaxation time of 1.38×10^{6} m/sec,[47] and 3.1×10^{-14} sec,[43] respectively, a particle diameter of 80 nm is obtained. Therefore, for particles larger than 80 nm across, bulk relaxation mechanisms dominate and bulk values for the complex dielectric constant are applicable. For smaller particles the surface effect should be dominant and modifications of the dielectric constant as described below may be more accurate. A particle 80 nm in diameter should have equal contributions from the bulk and "wall" relaxation mechanisms. The appropriate total relaxation time for free electrons in the particle is given by[29]

$$1/\tau = 1/\tau_0 + 2V_F/d . \tag{4}$$

Since the free-electron model and hence the variable τ were not used in the present calculations, the boundary or wall effect was introduced by modifying the bulk values of the dielectric constant of silver. From the free-electron model the real part of the dielectric constant is nearly independent of τ; however, the imaginary part is approximated as

$$\epsilon_2 \simeq \omega_p^2/\omega^3\tau , \tag{5}$$

TABLE I. Relative contributions to the total calculated scattered light intensity of various sized particles in those samples shown in Fig. 3. For each particle size group the calculated scattering cross section (at the resonance peak C_{max} is multiplied by the number of particles present in that size range (from Fig. 4). The product represents the relative contribution to the total spectrum (shown in Fig. 9) of that size group.

Sample (Fig. 3)	Particle diameter (nm)	(Number of particles (Fig. 4)) × (Greatest value (C_{max}) of calculated spectrum (nm^2)) = (Actual contribution (in Fig. 9))		
(a)	5	9000	0.1	900
	10	1700	7.0	11 900
	20	300	400	120 000
	40	90	23 000	2 070 000
	60	•••	120 000	•••
	80	•••	230 000	•••
	100	•••	277 000	•••
	120	•••	350 000	•••
(b)	5	3200	0.1	320
	10	1500	7.0	10 500
	20	220	400	88 000
	40	80	23 000	1 840 000
	60	10	120 000	1 200 000
	80	2	230 000	460 000
	100	0.2	277 000	55 400
	120	•••	350 000	•••
(c)	5	5000	0.1	500
	10	700	7.0	4 900
	20	185	400	74 000
	40	130	23 000	2 990 000
	60	63	120 000	7 560 000
	80	28	230 000	6 440 000
	100	10	277 000	2 770 000
	120	2	350 000	770 000

for typical values of the bulk plasma frequency ω_p and for ω in the optical region of the spectrum.

Figure 10 shows the spectra for the same particle distributions used in Fig. 9, but with the damping prescribed by Eqs. (4) and (5) included.[26] As the half-width of the resonance curves has increased, the peak of the resonance has decreased with respect to other regions of the scattered light spectrum which remain essentially unchanged. This has the consequence of making the rising scattered light intensity between 220 and 320 nm wavelengths a major feature of the scattered light spectrum. Such a magnitude of the scattered light intensity between 220 and 320 nm relative to the height of the resonance is in contradiction to the observed spectra.

It is actually not surprising that a model based on a free-electron gas should show some discrepancy for silver particles in this region of the spectrum. Even though the band gap in bulk silver is near 310 nm (4 eV), the absorption edge has a large effect on the real part of the dielectric function (ϵ_1) at slightly lower energies[48] where the particle resonance in silver occurs. In other words a significant contribution to the dielectric function in this spectral region comes from bound electrons[48] which, of course, are neglected by the simple model. Further, it is presumed in what follows that the bound electron distribution remains relatively unaffected by particle size.

By trial and error, the greatest amount of extra damping (simulated by increasing the values of ϵ_2) was determined such that reasonable agreement in the 220- and 320-nm wavelength region of the observed spectra was obtained (Fig. 11). This optimal amount of damping was approximately one half that predicted by the free-electron model, i.e., a particle 40 nm rather than 80 nm in diameter would have a relaxation time due to wall collisions equivalent to the bulk relaxation time. The general agreement between Figs. 2 and 11 is very good; the most significant discrepancy is again in the sharpness of the calculated spectra. Since Fig. 10 indicates that increasing damping cannot account for the width of the observed spectra, the conclusion from this analysis is that a difference between the observed and calculated spectra exists which is not corrected by adjusting

a parameter for the relaxation mechanisms.

It might be suggested that the observed broadening is due to larger particles in the system that somehow escaped being sampled. However, closer examination of the 220–320-nm region of the spectra (Fig. 2) shows that as the mean particle size increases, the slope of the rising scattered light intensity in this spectral region changes from slightly concave to convex. Therefore, the spectral region between 220 and 320 nm becomes quite useful since its relative magnitude is an indication of damping and its shape is an indication of mean particle size.

Another possible explanation for the widths of the observed spectra lies in the fact that the particles are not spheres but are irregular in shape. As previously mentioned, shape effects are generally difficult to address theoretically. One exception is for particles that are small compared to the wavelength, the polarizability of an arbitrarily shaped particle can be obtained by solving Laplace's equation (called the electrostatic mode method); resonances are determined in a similar way to that of Eq. (1). In terms of the dielectric function

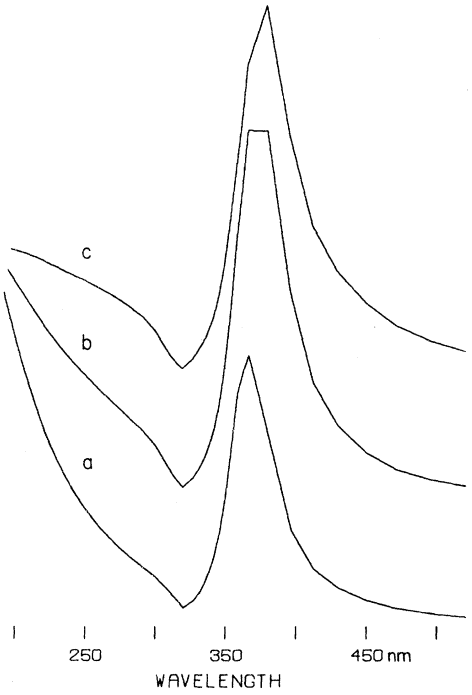

FIG. 10. Synthesized spectra obtained as in Fig. 9 except that the values of ϵ_2 have been increased to simulate electron damping due to particle boundaries. Amount of damping was determined from bulk values of the Fermi velocity and relaxation time. Resulting spectra have been normalized to the same maximum height and offset vertically. Offset, horizontal, and vertical scales match those in Fig. 2.

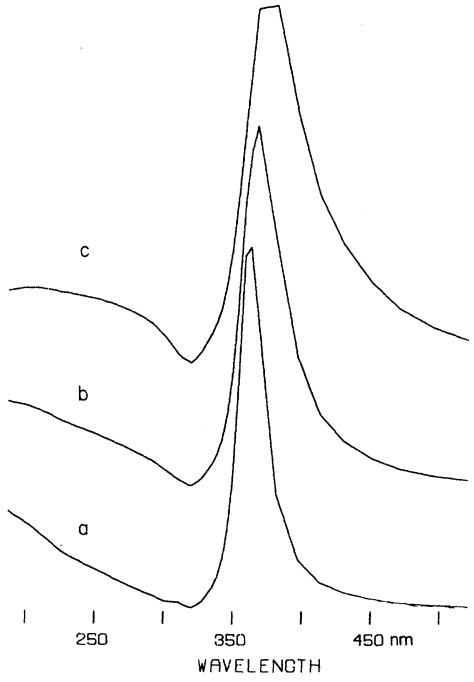

FIG. 11. Synthesized spectra obtained as in Fig. 9. Values of ϵ_2 have been increased from the bulk values only half as much as in Fig. 10, so that the damping effect of the particle boundaries on the spectra is less than in Fig. 10. Resulting spectra were normalized and offset.

this technique shows that resonances occur within the maximum of ϵ_2 on the lower energy side and the maximum of $(\epsilon_1^2+\epsilon_2^2)^{-1}$ on the higher-energy side[40] (i.e., when ϵ_1 is negative). For bulk silver this means resonances may occur at wavelengths from 330 to 1300 nm. Thus it is plausible that the long tail of the observed scattering resonance is due to resonance scattering of particles whose shapes deviate significantly from spherical. Another possible explanation for the lack of agreement is that while values of ϵ_2 were changed to simulate small particle damping, no attempt was made to derive ϵ_1 again from a Kramers-Krönig analysis for complete consistency.[41] The effect on ϵ_1 of increasing ϵ_2 is expected to be small, but would shift the resonance peak to longer wavelengths.

CONCLUSIONS

The severe decrease in scattering intensity with decreasing particle size was not fully appreciated until after the calculations were started. In Table I the maxima or peak values of the calculated spectra (C_{max}) of spheres of various diameters

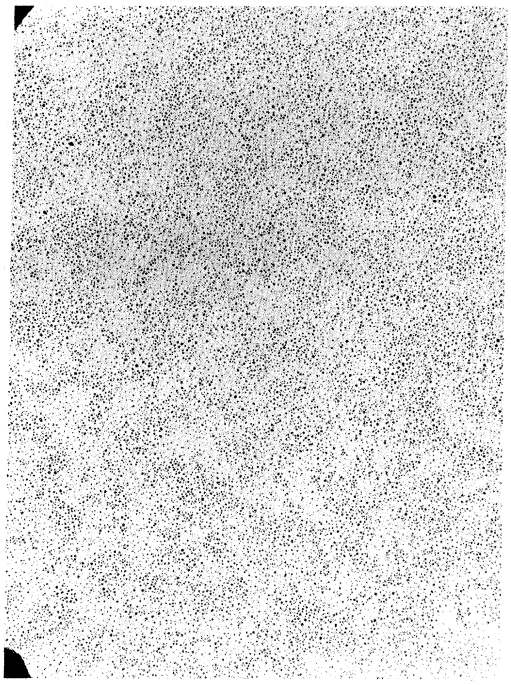

FIG. 12. Silver-particle samples collected at low pressure and close to the central flow stream. Particle diameters range from 2 to 18 nm.

are listed. It is seen that for particles smaller than 60 to 40 nm in diameter the scattering intensity decreases very rapidly with decreasing size (approximately as d^6). Consequently just a few very large particles will contribute as much to the total scattered light intensity as many smaller particles.

While observation of absorption by particles is experimentally more difficult, the absorption cross section may not change appreciably for the same range of particle sizes over which the scattering cross section changes several orders of magnitude.[29] Therefore, in retrospect, scattered light measurements were perhaps a poor choice for demonstrating the observed uniformity of particles such as illustrated in Fig. 12. Such samples were observed frequently (under conditions of lower chamber pressure), and the entire sampler grid was covered uniformly.

However, the light scattering results do illustrate the empirical limitations of using a spherical particle model when in fact deviations from spherical shape exist. It is of practical interest that a spherical model accurately predicted the general characteristics of the scattered light spectra, and to know the extent of the differences between spectra calculated for spheres and spectra obtained from real particles.

---

*Work supported in part by NSF Grant No. MPS-74-22714.

†Present address: Naval Research Laboratory, Washington, D. C.

[1]G. Mie, Ann. Phys. 25, 377 (1908).
[2]L. Harris, D. Jeffries, and B. M. Siegel, J. Appl. Phys. 19, 791 (1948).
[3]L. Harris, D. Jeffries, and B. M. Siegel, J. Opt. Soc. Am. 38, 582 (1948).
[4]L. Harris, D. Jeffries, and B. M. Siegel, J. Chem. Phys. 18, 261 (1950).
[5]K. Kimoto, Y. Kamiya, M. Nonoyama, and R. Uyeda, Jpn. J. Appl. Phys. 2, 702 (1963).
[6]A. Tasaki, S. Tomiyama, S. Iida, N. Wada, and R. Uyeda, Jpn. J. Appl. Phys. 4, 707 (1965).
[7]K. Kimoto and I. Nishida, J. Phys. Soc. Jpn. 22, 940 (1967).
[8]N. Wada, Jpn. J. Appl. Phys. 6, 553 (1967).
[9]K. Kimoto and I. Nishida, Jpn. J. Appl. Phys. 6, 1047 (1967).
[10]T. Tanaka and N. Tamagawa, Jpn. J. Appl. Phys. 6, 1096 (1967).
[11]N. Wada, Jpn. J. Appl. Phys. 7, 1287 (1968).
[12]T. Fujita, K. Ohshima, and N. Wada, J. Phys. Soc. Jpn. 27, 1459 (1969).
[13]K. Kusaka, N. Wada, and A. Tasaki, Jpn. J. Appl. Phys. 8, 599 (1969).
[14]T. Fujita, K. Ohshima, and N. Wada, J. Phys. Soc. Jpn. 29, 797 (1970).
[15]S. Kobayashi, T. Takahashi, and W. Sasaki, J. Phys. Soc. Jpn. 31, 1442 (1971).
[16]S. Yatsuya, R. Uyeda, and Y. Fukano, Jpn. J. Appl. Phys. 11, 408 (1972).
[17]C. Kaito, K. Fujita, and H. Hashimoto, Jpn. J. Appl. Phys. 12, 489 (1973).
[18]S. Yatsuya, S. Kasukabe, and R. Uyeda, Jpn. J. Appl. Phys. 12, 1675 (1973).
[19]S. Takjo, S. Kobayashi, and W. Sasaki, J. Phys. Soc. Jpn. 35, 712 (1973).
[20]E. O. Hogg and B. G. Silbernagel, J. Appl. Phys. 45, 593 (1974).
[21]S. Yatsuya, K. Mihama, and R. Uyeda, Jpn. J. Appl. Phys. 13, 749 (1974).
[22]R. Monot, A. Chatelain, and J. P. Borel, Phys. Lett. A 34, 57 (1971).
[23]M. Rappaz and F. Faes, J. Appl. Phys. 46, 3273 (1975).
[24]D. M. Mann and H. P. Broida, J. Appl. Phys. 44, 4950 (1973).
[25]J. B. West, R. S. Bradford, Jr., J. D. Eversole, and C. R. Jones, Rev. Sci. Instrum. 46, 164 (1975).
[26]J. D. Eversole, Ph.D. thesis (University of California, Santa Barbara, 1975) (unpublished).
[27]S. E. Johnson, K. Sakurai, and H. P. Broida, J. Chem. Phys. 52, 6441 (1970).
[28]C. J. Duthler, S. E. Johnson, and H. P. Broida, Phys. Rev. Lett. 26, 1236 (1971).

[29]W. T. Doyle and A. Agarwal, J. Opt. Soc. Am. 55, 305 (1965).
[30]J. D. Eversole and H. P. Broida, J. Appl. Phys. 45, 596 (1974).
[31]S. Yamaguchi, J. Phys. Soc. Jpn. 15, 1577 (1960).
[32]S. Yamaguchi, J. Phys. Soc. Jpn. 17, 184 (1962).
[33]R. H. Doremus, J. Appl. Phys. 35, 3456 (1964).
[34]R. H. Doremus, J. Chem. Phys. 42, 414 (1965).
[35]D. C. Skillman and C. R. Berry, J. Chem. Phys. 48, 3297 (1968).
[36]U. Kreibig and P. Zacharias, Z. Phys. 231, 128 (1970).
[37]S. Yoshida, S. Yamaguchi, and A. Kinbara, J. Opt. Soc. Am. 62, 1415 (1972).
[38]R. W. Cohen, G. D. Cody, M. D. Coutts, and B. Abeles, Phys. Rev. B 8, 3689 (1973).
[39]R. W. B. Pearse and A. G. Gaydon, *The Identification of Molecular Spectra 3rd Ed.* (Wiley, New York, 1963), pp. 53.
[40]D. P. Gilra, Ph.D. thesis (University of Wisconsin, 1972) (unpublished), pp. 123–26.
[41]U. Kreibig and P. Zacharias, Z. Phys. 234, 307 (1970).
[42]M. A. Smithard and M. Q. Tran, Helv. Phys. Acta 46, 869 (1974).
[43]P. B. Johnson and R. W. Christy, Phys. Rev. B 6, 4370 (1972).
[44]H. J. Hagemann, W. Gudat, and C. Kunz, *Optical Constants from the Far Infrared to the X-Ray Region* (DESY SR-74/7, 2 Hamburg 52, Notkestieg 1, Germany, 1974).
[45]M. Kerker, *The Scattering of Light and Other Electromagnetic Radiation* (Academic, New York, 1969).
[46]H. C. Van De Hulst, *Light Scattering by Small Particles* (Wiley, New York, 1957).
[47]C. Kittel, *Introduction to Solid State Physics, 3rd Ed.* (Wiley, New York, 1976), pp. 208.
[48]H. Ehrenreich and H. R. Philipp, Phys. Rev. 128, 1622 (1962).

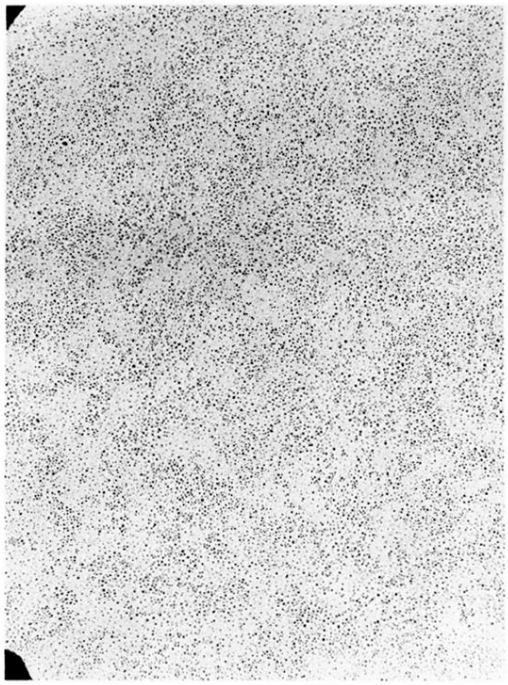

FIG. 12. Silver-particle samples collected at low pressure and close to the central flow stream. Particle diameters range from 2 to 18 nm.

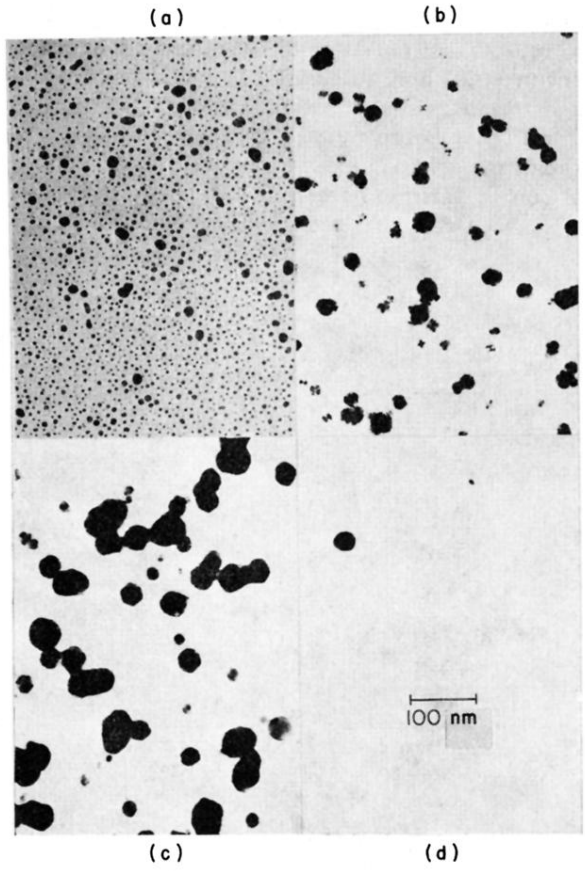

FIG. 3. Pressure dependence of samples of silver particles. Four samples were obtained under the same conditions as the spectra shown in Fig. 2, with (a) taken at the lowest pressure (0.09 kPa), (b) at 0.16 kPa, (c) at 0.31 kPa, and (d) at 0.99 kPa. Scale indicated in (d) applies to all four photographs. Samples were obtained at approximately the same location in the observation chamber from collection grids exposed for about 10 sec. Owing to the high contrast required for reproduction some of the smaller particles do not show up. Particles shown in (a) have rounded shapes because of a long period of storage in air.